

# Human-Object Interaction from Human-Level Instructions

Zhen Wu      Jiaman Li      Pei Xu      C. Karen Liu  
Stanford University  
{zhenwu, jiamanli, peixu, karenliu}@cs.stanford.edu



Figure 1. Given human-level instructions (top), we first use a diffusion-based motion generator to synthesize natural full-body human motion, finger motion, and object motion to accomplish the task (middle). Next, we employ a physics-based tracking method to imitate the generated interactions which produces physically plausible interactions (bottom). Please refer to our [project page](#) for more results.

## Abstract

*Intelligent agents must autonomously interact with the environments to perform daily tasks based on human-level instructions. They need a foundational understanding of the world to accurately interpret these instructions, along with precise low-level movement and interaction skills to execute the derived actions. In this work, we propose the first complete system for synthesizing physically plausible, long-horizon human-object interactions for object manipulation in contextual environments, driven by human-level instructions. We leverage large language models (LLMs) to interpret the input instructions into detailed execution plans. Unlike prior work, our system is capable of generating detailed finger-object interactions, in seamless coordination with full-body movements. We also train a policy to track generated motions in physics simulation via reinforcement learning (RL) to ensure physical plausibility of the motion. Our experiments demonstrate the effectiveness of our system in synthesizing realistic interactions with diverse objects in complex environments, highlighting its potential for real-world applications.*

## 1. Introduction

Synthesizing physically plausible, long-horizon, human-object interactions in contextual environments is crucial

for applications in computer graphics, embodied AI, and robotics. When given human-level language instructions, intelligent agents should be able to comprehend these high-level commands and map them to executable action sequences. For instance, when instructed to set up a workspace, an agent must understand the abstract concept of “workspace”, identify the relevant furniture and objects in the room, and translate this concept into a series of concrete actions, such as moving and orienting a desk, placing a chair nearby, and positioning a monitor on the desk. In addition to understanding the instructions, the agent must execute actions that lead to realistic and functional human movements, including navigating cluttered spaces, manipulating various objects for the task, and appropriately releasing them after use.

Prior research has made significant progress in synthesizing human-scene interactions using large language model (LLM) planners [60]. However, most of these interactions have been limited to static objects without hand manipulation. Some studies [25] have demonstrated the manipulation of dynamic objects, but the resulting interactions still lack realistic finger movements. Recently, physics-based RL policies has demonstrated promising results in human-object interactions [32, 55]. However, generating long-horizon motions that interact with various objects in a scene-aware manner remains an ongoing challenge. Build upon these prior work, we introduce the first complete system capable

of synthesizing physically accurate, long-horizon human-object interactions with synchronous full-body and intricate finger movements, from human-level language instructions.

Synthesizing coordinated full-body and finger movements from human-level instructions presents two main challenges. First, human-level instructions typically provide only a high-level task outline, requiring common sense and world knowledge to translate them into precise object arrangements and detailed execution plans. Second, existing datasets with paired full-body and finger motion data are limited to interactions with small objects and lack locomotion during object manipulation [8, 46]. Although a recent dataset [26] includes locomotion and manipulation for large objects, it lacks detailed finger movements due to the difficulty of capturing both modalities simultaneously.

To tackle the challenge of comprehending human-level instructions, we utilize the latest advancements in LLMs, which are highly effective in interpreting high-level commands [29, 36]. However, LLMs are not well-suited for directly predicting precise scene layouts, such as the exact positions and orientations of objects [1, 16]. Instead of prompting LLMs to directly specify object placements, we use object spatial relationships as intermediate representations and ask LLMs to derive these relationships. We then propose an algorithm to calculate the precise object poses based on these relationships.

For the low-level motion synthesis, we take the approach of modeling human motion from real-world human data. To address the lack of large-scale object manipulation datasets with synchronized full-body and finger motions, one could use two separate datasets to train a full-body manipulation model and another detailed finger manipulation model. However, simply fusing the two motions together will cause glaring artifacts due to the disagreement in two separately trained models. Our solution is to break this process into three steps. We first generate full-body and object motions without detailed fingers. The object motion and rough wrist poses provide guidance for generating contact-consistent finger motion in the second step. Finally, we generate full-body and object motions again conditioned on precise finger motions. This approach enables our framework to successfully produce synchronized object motion, full-body motion, and finger motions without requiring a dataset that includes all data modalities.

The generated motion, however, is not guaranteed to be physically accurate. To ensure physical plausibility, we further use reinforcement learning (RL) to track the generated motion in a physics simulator. Our method adopts an importance sampling technique to improve the training efficiency of long sequence tracking and supports tracking diverse interactions with multiple distinct objects within a single sequence.

We evaluate our method through extensive quantitative

and qualitative comparisons, as well as human studies, demonstrating that our approach outperforms all others. This underscores the effectiveness of our method and its potential for real-world applications.

## 2. Related Work

**Contextual Interaction Synthesis.** Recent work on modeling human-object interactions falls into two categories: interactions with static and dynamic objects. Synthesizing human motions in static 3D scenes has been extensively studied [2, 13, 14, 21, 56, 71]. Prior research has explored regression models [2, 14, 34, 51, 52] and diffusion models [18, 21, 57, 68] to generate human motions interacting with 3D scenes, such as sitting on a chair or lying down on a sofa. Some studies have also explored reinforcement learning methods to generate physically plausible human motions [15, 60, 73]. These works focus on static objects, whereas our work focuses on dynamic interactions.

There has been increasing attention on synthesizing human-object interactions with dynamic objects [6, 38, 58, 64]. OMOMO [26] collected a dataset for dynamic human-object interactions and proposed a framework to synthesize human motions from object motions. CHOIS [25] synthesizes interactions in 3D scenes from text and sparse way-points. Despite these advancements, all of these works focus on full-body human motion generation without detailed finger motions. In this work, we aim to generate synchronized object motions, human motions, and finger motions.

**Hand-Object Interaction Synthesis.** Hand-object interaction synthesis has been extensively explored. In the realm of static pose generation, traditional methods often rely on physics-based control or optimization techniques to generate grasp candidates [28, 41, 44]. Some recent work leverages deep learning to directly estimate hand grasps from extensive interaction datasets [3, 5, 8, 19, 23, 46]. Beyond static grasping, another line of work also explores dynamic object manipulation [31, 67, 70].

Recent works further explore integrating whole-body motion and hand motion [47–49, 59]. IMoS [10] generates hand-object interaction using paired human motion and hand motion, while [4] leverage reinforcement learning to achieve physically plausible motion. However, these methods are constrained to manipulate small-sized objects in the GRAB dataset [46], unable to generalize to large objects. In this work, we aim to generate realistic full-body and finger motions for manipulating large objects. Since no such paired dataset exists, we leverage DexGraspNet [53] to generate realistic grasp poses, train a conditional diffusion model on GRAB [46] to generate approaching and releasing finger motions, and then integrate these with our full-body motion generation.

**Physics-Based Motion Synthesis.** Physics-based methods control a simulated character to perform motion in a simulator, ensuring the physical realism of the generated motion. To make the motion more natural, many approaches leverage motion capture data to produce movements that match the style of the data [30, 38–40]. DeepMimic [39] proposes to track motion capture data using RL. Subsequent works [40, 62] leverage generative adversarial networks (GANs) to learn motion styles. Recent research also explores this approach for human-object interactions, such as playing musical instruments [54, 63] or playing soccer [61]. PhysHOI [55] learns basketball-playing skills from human demonstrations. OmniGrasp [32] enables a character to grasp and move an object along a specified object trajectory. In this work, we leverage RL to track generated kinematic motion, successfully producing long-horizon motions that interact with various objects.

**LLM-based Planning.** LLMs have been widely used in reasoning, planning tasks [7, 16, 17, 50, 69] for their high-level planning capabilities. They have also been adopted in motion synthesis tasks [60, 64, 66, 72]. UniHSI [60] uses LLMs to extract action plans in a chain-of-contact format, guiding a low-level controller to synthesize corresponding motions. InterDreamer [64] employs LLMs to identify object parts that humans interact with and uses this information to retrieve initial human poses. In this work, we leverage LLMs to translate abstract human-level instructions into target scene maps and detailed execution plans, which guide the low-level interaction synthesis.

### 3. System Overview

Given a human-level instruction and a scene description, we develop a system that generates synchronized human motion and object motion to accomplish the task. An overview of our system is depicted in Fig. 2. The system consists of a high-level planner, a low-level motion generator, and a physics tracker. The high-level planner leverages LLMs to reason about instructions and the scene description, generating a *scene map* along with a detailed *execution plan*. The scene map specifies the desired positions and orientations of the objects, while the execution plan outlines the steps to interact with these objects. The low-level motion generator unites conditional diffusion models trained on separate datasets for full body motion and dexterous hand motion, producing synchronous object and human movements. The physics tracker then uses RL to track the generated motion in a physics simulator, ensuring physical plausibility.

### 4. High-Level LLM Planner

Inputs to the high-level planner consist of an initial scene description and human-level instructions. The scene descrip-

tion includes a list of objects in a 3D scene and their layout, while the human-level instruction describes a task that requires grounded reasoning based on world knowledge and common sense. For example, the instruction “I want to do yoga in front of the TV” implies that any obstacles in front of the TV should be moved elsewhere.

Outputs of the high-level planner comprise the scene map and the execution plan. The scene map specifies the target position  $p$  and orientation  $q$  for each object  $o$  that requires movement, represented as  $\{\{o_1, p_1, q_1\}, \dots, \{o_n, p_n, q_n\}\}$ . The execution plan is a sequence of text actions associated with objects in the scene map. For example, “lift the monitor, move the monitor, put down the monitor”.

#### 4.1. Scene Map Generation

To obtain a reliable scene map, inspired by recent works in room layout generation [1, 65], we first instruct LLMs to reason about spatial relationships of the objects as an intermediate representation from which the 3D positions and orientations of the objects are calculated subsequently. We define the following relation functions to capture spatial relationships, with flexibility to include additional relationships if needed.

1. `on(object1, object2)`.
2. `adjacent(object1, object2, direction, distance)`.
3. `facing(object1, object2)`.

For example, if a monitor needs to be put on the table facing the chair, we can use `on(monitor, table)` and `facing(monitor, chair)` to describe its pose. If a table is positioned 1 meter to the north of the door, we can use `adjacent(table, door, north, 1)` to describe the relationship. We prompt LLMs to generate the spatial relationships of the objects according to the given instruction.

Given the spatial relationships, we propose an algorithm to calculate the 3D positions of each object in the scene. The orientations of objects, enforced by “facing” relations, will be addressed in the subsequent step.

The algorithm first constructs a scene graph [22] to organize the objects (nodes) and their spatial relationships (edges), which are directional, pointing from `object2` to `object1`. The algorithm employs a method similar to topological sorting, assuming no cycles are present in the graph. The scene graph is initialized by visiting the nodes associated with static objects and setting their 3D positions as the given values. In each iteration, the algorithm looks for a new node whose 3D position has not been determined but all its predecessors have. By calculating an offset from the predecessors’ known positions, we can determine the position of the new node. For example, if object  $o_1$  is “on” object  $o_2$ , then  $o_1$ ’s height is set to match the top surface of  $o_2$ , while the horizontal position is sampled within the



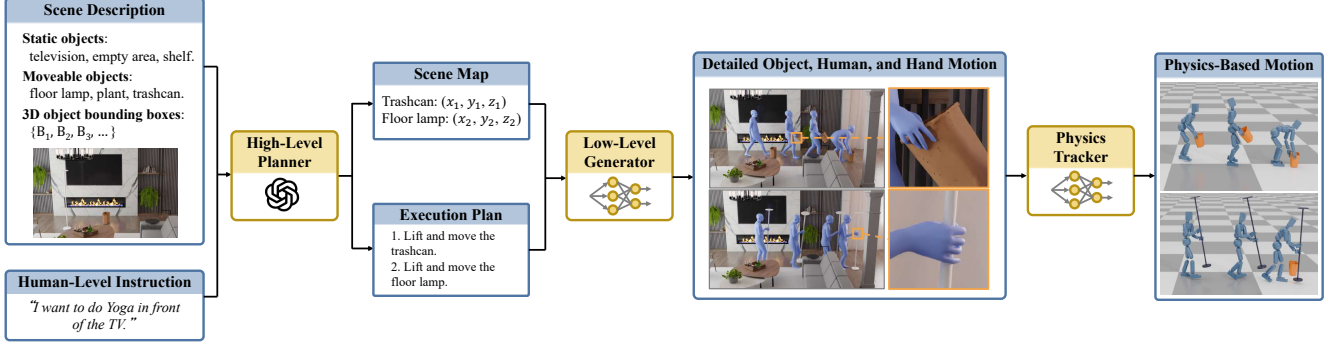


Figure 2. Our system takes the scene description and human-level instruction as input and uses a high-level planner to obtain the scene map and a detailed execution plan. The low-level motion generator then generates synchronized object motion, full-body human motion, and finger motion. Finally, the physics tracker uses RL to track the generated motion, producing physically plausible motion.

horizontal range of  $o_2$ . If  $o_1$  is “adjacent” to  $o_2$ , we use the direction and distance given by the LLMs as the offset. We have included pseudo-code in the supplementary material.

To compute the orientation enforced by `facing`( $o_1$ ,  $o_2$ ), we rotate the canonical direction of  $o_1$  in its own local frame to align with the vector from the position of  $o_1$  to the position of  $o_2$ . The canonical direction of each object is part of the input 3D geometry information.

## 4.2. Execution Plan Generation

After determining the scene map, the planner must specify the interaction order with each object to ensure natural motion. For instance, if a vase is on a table, the vase should be moved before the table. LLMs are asked to generate this action sequence in a natural order and provide reasoning for it. The resulting execution plan consists of textual actions,  $\{l_1, l_2, \dots, l_T\}$ , where each action  $l_t$  defines interaction involving one object. Each  $l_t$  serves as the textual input for the low-level generator, following the format: “lift the *object*, move the *object*, put down the *object*”. This format is designed to closely match the textual style of the training dataset of the low-level generator.

With the scene map and execution plan in place, an A\* planner generates collision-free paths to execute the plan. The path is a series of 2D waypoints in the scene, which then serve as inputs for the low-level motion generator.

## 5. Low-Level Motion Generator

Given the waypoints and textual instructions generated by the high-level planner, the low-level motion generator executes an interaction module and a navigation module sequentially to generate long-horizon human-object interaction motions.

### 5.1. Background: Conditional Diffusion Model

The diffusion model involves a forward diffusion process and a reverse diffusion process. Starting from clean data  $x_0$ , noise is progressively introduced until, after  $N$  steps, the

data becomes approximately  $x_N \sim \mathcal{N}(0, I)$ . The denoising network is trained to reverse this process so that sampling a noise  $x_N$  and applying  $N$  denoising steps yields the clean data representation  $\hat{x}_0$ . Each denoising step is defined as

$$p_\theta(x_{n-1}|x_n, c) := \mathcal{N}(x_{n-1}; \mu_\theta(x_n, n, c), \sigma_n^2 I), \quad (1)$$

where  $p_\theta$  represents a neural network,  $c$  represents the conditions,  $\mu_\theta(x_n, n, c)$  represents the learned mean,  $\sigma_n^2$  denotes a fixed variance. The training loss is defined as  $\mathcal{L} = \mathbb{E}_{x_0, n} \|\hat{x}_\theta(x_n, n, c) - x_0\|_1$ .

### 5.2. Interaction Module

We introduce a multi-stage interaction module that synthesizes synchronized full-body, finger, and object motion, as shown in Fig. 3. The first stage, *CoarseNet*, generates initial human and object motions without detailed finger movement. Recognizing that finger poses typically remain static during interaction, the second stage generates a *grasp* pose based on the initial results. Then *RefineNet* re-generates the human and object motions to seamlessly align with the optimized grasp pose. Finally, *FingerNet* generates smooth finger motions for approaching and releasing the object, completing the interaction sequence.

#### 5.2.1. CoarseNet

Given the initial human and object poses, waypoints, and final object pose, along with a text instruction, CoarseNet generates synchronized human motion and object motion. This is achieved using a pre-trained diffusion model CHOIS [25].

**Data Representation.** We denote human motion as  $H \in \mathbb{R}^{T \times D}$ , where  $T$  represents the sequence length and  $D$  represents the dimension of the human pose. Each  $H_t$  includes global joint positions and 6D rotations [74], excluding finger joints. Object motion  $O \in \mathbb{R}^{T \times 12}$  includes the object’s global position and rotation matrix. CoarseNet predicts human motion, object motion, and contact labels  $L \in \mathbb{R}^2$  for both hands, resulting in  $x = \{H, O, L\}$ .

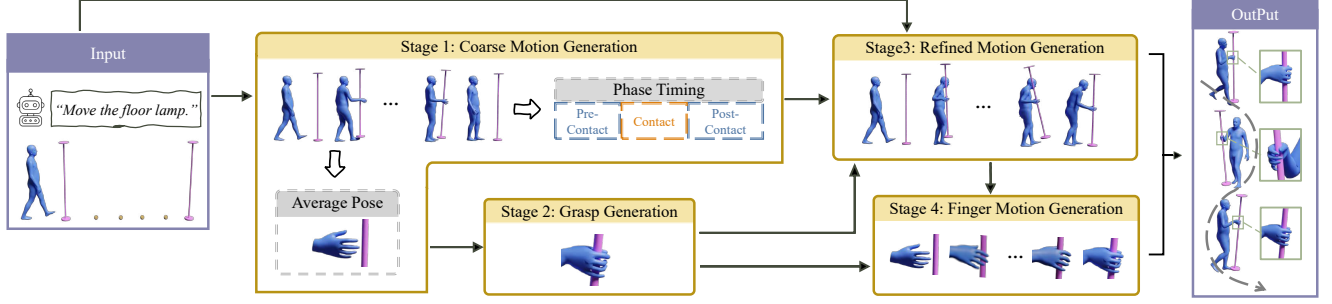


Figure 3. The interaction module consists of four stages. Starting with the initial human and object poses, waypoints, final object pose, and a text instruction, the first stage generates coarse object and human motion. The relative wrist pose from this motion is then used to generate a valid grasp pose. Using this as a condition, the next stage re-generates the motion to align with the grasp constraint. Finally, the finger motion generation module produces finger motions during the approach and release of objects.

The input condition is represented as  $c = \{S, G, T\}$ .  $S \in \mathbb{R}^{T \times (D+12)}$  is a masked motion data representation. It includes the human and object pose in the first frame, the object pose in the last frame, and 2D waypoints sampled every 30 frames. Any remaining entries in  $S$  are padded with zeros. The object geometry  $G$  represents the BPS representation [42] to encode object geometry, and  $T$  refers to the text embeddings extracted using CLIP [43].

**Segmenting Contact Phases.** We segment the generated interaction sequence into *pre-contact*, *contact*, and *post-contact* phases based on the predicted contact labels  $L$ . The contact phase is determined separately for each hand, dividing the model output  $x_{\text{coarse}}$  into  $x_{\text{pre-contact}} \oplus x_{\text{contact}} \oplus x_{\text{post-contact}}$ . We then compute the average wrist pose  $w$  from  $x_{\text{contact}}$ , serving as input for the next stage.

### 5.2.2. Grasp Pose Generation

The second stage generates the finger pose for the contact phase using a state-of-the-art grasp pose generation method [53]. Given an object, wrist pose  $w$  and rest finger pose, an optimization is conducted to generate a physically plausible grasp pose. We modified [53] to fit our needs by: (1) increasing the object surface sample points from 2,000 to 20,000 to maintain sample density for larger objects and (2) omitting the force closure term for tasks involving both hands, such as carrying a box, where stability doesn't solely rely on a single hand.

The optimized grasp pose is denoted by  $\hat{g} = (\hat{w}, \hat{\theta})$ , where  $\hat{w}$  is the optimized wrist pose, and  $\hat{\theta}$  is the finger pose. This grasp pose  $\hat{g}$  is maintained throughout the contact phase. However, as CoarseNet's generated motion may not fully align with  $\hat{w}$ , we introduce RefineNet to address this misalignment.

### 5.2.3. RefineNet

The goal of RefineNet is to re-generate human-object interaction motions that align with the optimized grasp pose  $\hat{g}$ . We adopt a conditional diffusion model based on CoarseNet, adding two conditions: *wrist-object relative pose* to align

the wrist with  $\hat{w}$  and *object static* to keep the object stationary during non-contact phases. RefineNet's input condition,  $c_r = \{W, S_r, G, T\}$ , includes  $G$  and  $T$  from CoarseNet, with  $W$  and  $S_r$  detailed as follows.

**Wrist-Object Relative Pose Condition.** The condition  $W \in \mathbb{R}^{T \times 18}$  represents the position and 6D rotation of both wrists in the object's frame, including only contact-phase wrist poses, with other entries set to zero.

**Object Static Condition.** In CoarseNet, the masked motion condition  $S$  was zero-padded except at the start, end, and waypoints. RefineNet uses contact phase information from CoarseNet to adjust  $S$  to  $S_r$ , assigning a static object pose in pre-contact and post-contact frames.

**Wrist-Object Relative Pose Loss.** We incorporate an additional loss to enforce the wrist-object relative pose condition. We sample 100 points  $K_{\text{rest}} \in \mathbb{R}^{100 \times 3}$  uniformly on the rest object's surface and pre-calculate their positions in both wrists' coordinate frames, denoted as  $K_w \in \mathbb{R}^{2 \times T \times 100 \times 3}$ . At each time step, we compute the points' positions in the wrist frame,  $\hat{K}_w$ , using the predicted orientations and positions of the object and wrist,  $R_o, T_o, R_w, T_w$ :

$$K_{\text{global}} = R_o K_{\text{rest}} + T_o, \quad (2)$$

$$\hat{K}_w = R_w^{-1} (K_{\text{global}} - T_w). \quad (3)$$

The loss is computed as:

$$\mathcal{L}_{\text{relative}} = \sum_{t=1}^T L_t \left\| \hat{K}_{w,t} - K_{w,t} \right\|_1, \quad (4)$$

where  $L_t$  represents the contact labels, masking out the loss when the hand and object are not in contact.

**Post-Processing.** RefineNet generates human-object motions that align closely with input conditions, though minor adjustments may be required. To refine alignment, we apply post-processing: replacing object poses in pre- and

post-contact phases with static poses and recalculating wrist trajectories during the contact phase based on object motion and the optimized wrist pose  $\hat{w}$ . Additional implementation details are in the supplemental materials.

#### 5.2.4. FingerNet

In this stage, we generate finger motions for the pre-contact and post-contact phases to create natural transitions between the rest and grasp poses, forming a complete interaction sequence along with predictions in prior stages. Given the start and end finger poses and the wrist trajectory in between, we employ a conditional diffusion model to predict the finger motions denoted as  $F \in \mathbb{R}^{T \times D'}$ , representing local 6D rotations [74].

The model is conditioned on  $c_f = \{P, F_s, F_e\}$ , where  $P$  captures spatial hand-object relationships and  $F_s, F_e$  are the start and end finger poses. Following prior work [48, 70],  $P \in \mathbb{R}^{T \times 100}$  is computed by sampling 100 palm-side mesh vertices and measuring their closest distances to the object, with the finger pose set to mean pose when calculating  $P$ .

#### 5.3. Navigation Module

To generate long sequences of interactions with multiple objects, the human needs to navigate through the scene based on waypoints. We adopt a conditional diffusion model to generate human navigation motion  $H \in \mathbb{R}^{T \times D}$ . The input conditions consist of the initial human pose, 2D waypoints, and waypoint orientations (expressed as normalized direction vectors) to maintain consistent facing directions. Smooth transitions between the interaction and navigation modules are achieved by using the final pose of one module as the starting pose for the next.

### 6. Physics Tracker

After obtaining a sequence of kinematic motions, we train a tracking policy using reinforcement learning to control a physically simulated character that imitates these motions. This approach helps eliminate artifacts (e.g., hand-object penetration and foot sliding) in the kinematic motions and ensures the physical plausibility of the generated results.

We use PPO [45] as the backbone reinforcement learning algorithm, and adopt an importance sampling strategy to facilitate the tracking of long motion sequences involving interactions with multiple objects. Policies trained by our approach can accurately track the kinematics motions, enabling the character to grasp and move distinct objects along the generated trajectories. Implementation and training details for the physics tracker are provided in the supplementary materials.

### 7. Experiment

We conduct extensive evaluation to assess the overall performance of our system, as well as each individual component.

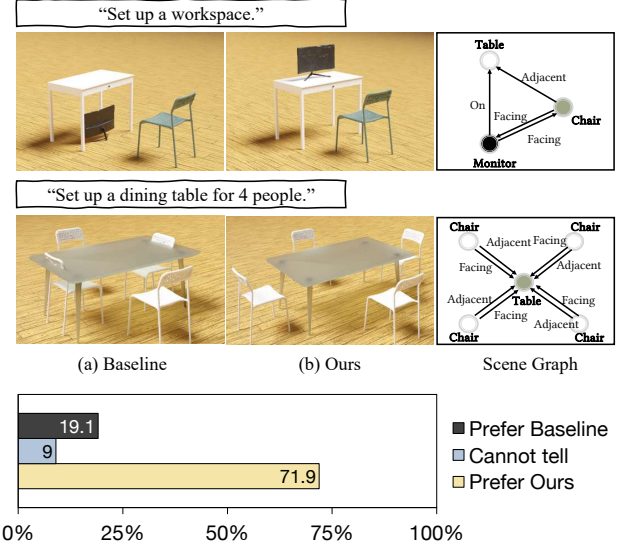


Figure 4. Comparison between (a) the baseline and (b) our high-level planner. The baseline generates an incorrect monitor position and orientation, and places the chair in a position that intersects with the table. The human perception study results (bottom) show that the majority of participants preferred our results.

We use quantitative metrics and user perception studies to evaluate our results compared to the baselines. We also conduct ablation studies to analyze the effects of each system module. We present the key results in this section and highly recommend readers refer to the supplementary video and documents for more detailed results and descriptions of the studies.

#### 7.1. Evaluation of High-Level Planner

The core component of the high-level planner is the scene map calculation. To assess its effectiveness, we quantitatively measure the geometric accuracy of the resulting plans and conduct a human perception study. For evaluation, we compare our method to a baseline that uses LLMs to directly predict object positions and orientations. We design 25 human-level instructions covering common everyday tasks for assessment, using OpenAI’s GPT-4o [35] for both our method and the baseline.

For geometric accuracy, we measure the proportion of objects with positional ( $PE_p$ ) or orientation errors ( $PE_o$ ) in the scene. Positional errors include objects placed at incorrect heights or with penetration into other objects, while orientation errors refer to objects being directed in the wrong direction. The results, shown in Tab. 2, demonstrate that our method outperforms the baseline by a large margin. A qualitative comparison is presented in the upper part of Fig. 4,

Table 2. Comparison of geometric accuracy between our method and the baseline.

|          | $PE_p \downarrow$ | $PE_o \downarrow$ |
|----------|-------------------|-------------------|
| Baseline | 21.9%             | 12.5%             |
| Ours     | <b>3.1%</b>       | <b>1.6%</b>       |

The results, shown in Tab. 2, demonstrate that our method outperforms the baseline by a large margin. A qualitative comparison is presented in the upper part of Fig. 4,



| Method          | Condition           | Human Motion                 |                 |                            | Interaction               |                          |               |                 | GT Difference      |                             |                             |
|-----------------|---------------------|------------------------------|-----------------|----------------------------|---------------------------|--------------------------|---------------|-----------------|--------------------|-----------------------------|-----------------------------|
|                 | $T_{xy} \downarrow$ | $H_{\text{feet}} \downarrow$ | FS $\downarrow$ | $C_{\text{prec}} \uparrow$ | $C_{\text{rec}} \uparrow$ | $C_{\text{F1}} \uparrow$ | CC $\uparrow$ | IV $\downarrow$ | MPJPE $\downarrow$ | $T_{\text{obj}} \downarrow$ | $O_{\text{obj}} \downarrow$ |
| CNet+GRIP [48]  | 3.58                | <b>2.50</b>                  | 0.45            | 0.90                       | 0.64                      | 0.70                     | 3.99%         | 49.00           | 14.33              | 11.55                       | 0.93                        |
| CNet            | 3.26                | 2.68                         | 0.43            | 0.91                       | 0.81                      | 0.84                     | 3.54%         | 48.56           | <b>14.32</b>       | <b>10.56</b>                | 1.06                        |
| C+RNet          | <b>2.81</b>         | 2.89                         | <b>0.33</b>     | <b>0.91</b>                | <b>0.95</b>               | <b>0.92</b>              | 3.84%         | 24.78           | 15.96              | 12.57                       | <b>0.73</b>                 |
| C+R+FNet (ours) | <b>2.81</b>         | 2.89                         | <b>0.33</b>     | <b>0.91</b>                | <b>0.95</b>               | <b>0.92</b>              | <b>5.53%</b>  | <b>19.06</b>    | 15.96              | 12.57                       | <b>0.73</b>                 |

Table 1. Interaction synthesis on the FullBodyManipulation dataset [26]. Our full model achieves superior interaction quality compared to all others.

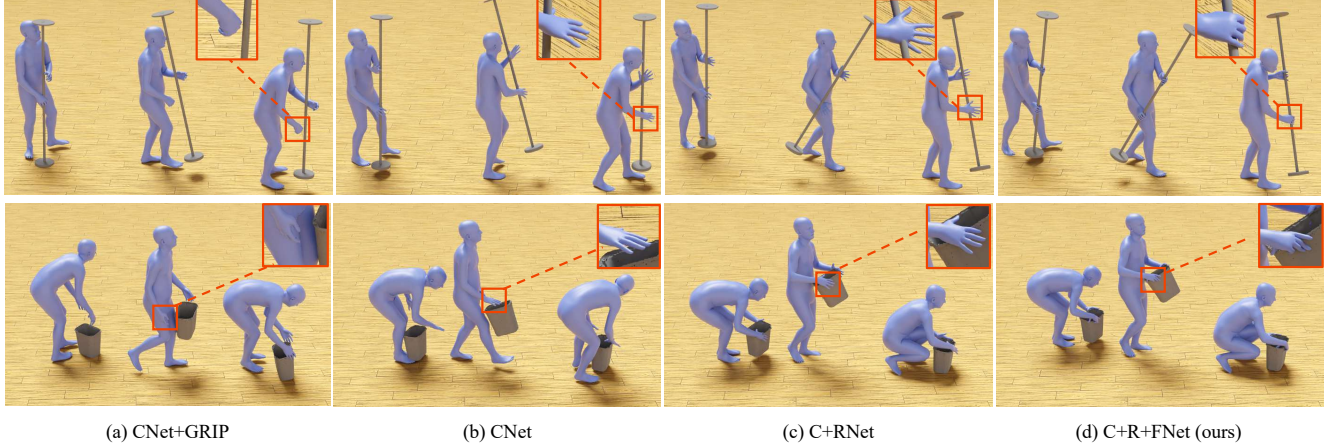


Figure 5. Qualitative comparisons of each method. All baselines and ablations fail to produce precise hand and finger motions, while our method generates natural hand-object interactions.

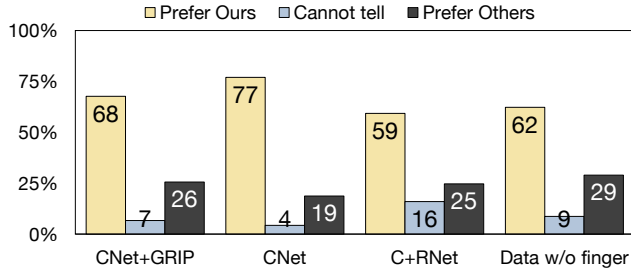


Figure 6. Comparison of our full model and baseline models through human perception studies.

where the baseline generates incorrect object positions and orientations, while our method produces more reasonable layouts.

We also conducted a human perception study, with results presented in the lower part of Fig. 4. Each pair was reviewed by 20 Amazon Mechanical Turk (AMT) workers. They were asked to choose the scene that was more reasonable and consistent with the given instruction. The majority of participants preferred our method.

## 7.2. Evaluation of Low-Level Motion Generator

**Datasets.** CoarseNet and RefineNet are trained on the Full-BodyManipulation dataset [26], which includes 10 hours of human-object interaction with 15 objects but lacks finger

motion. FingerNet uses the GRAB dataset [46], containing full-body and finger motion for 10 subjects with 51 objects. The navigation module is trained on HumanML3D [12], featuring 28 hours of diverse motions with language descriptions. For all datasets, we follow standard data partitioning from prior work [12, 26, 46].

**Evaluation Metrics.** Following prior work [25], we evaluate our approach from various aspects. All distance errors are measured in centimeters. For condition matching, we report the waypoint following errors ( $T_{xy}$ ). For human motion quality, we report the foot sliding score (FS) and foot height ( $H_{\text{feet}}$ ). For interaction quality, we use contact precision ( $C_{\text{prec}}$ ), recall ( $C_{\text{rec}}$ ), and F1 score ( $C_{\text{F1}}$ ). To better assess finger-object interaction, we also report contact coverage (CC) – the percentage of hand points within -2mm to +2mm of the object surface – and intersection volume (IV), the overlap volume of hand and object meshes in  $\text{cm}^3$ , following [11]. For ground truth difference, we report the mean per-joint position error (MPJPE), object position error ( $T_{\text{obj}}$ ), and the object orientation error ( $O_{\text{obj}}$ ). We also conduct a human perception study to measure the motion quality.

**Baselines.** For generating full-body human motion, finger motion, and object motion from text, prior work [9, 27] trained models on GRAB [46] to predict motions for small-object manipulation. However, GRAB contains only small-

object manipulation data without locomotion, so models trained on it cannot generalize to scenarios involving large objects that require full-body coordination and locomotion. Moreover, the approach from [9, 27] is not applicable to the FullBodyManipulation dataset [26] used in our work, as this dataset lacks finger motions, making it infeasible to learn a model via direct supervision. Due to these differences, a directly comparable baseline does not exist. Thus, we establish our baseline by combining two complementary methods: CHOIS [25] (referred to as CoarseNet in our framework), which generates object motion and full-body motion from text, and GRIP [48], which refines arm movements and generates finger motions based on CHOIS’s output.

In addition, to evaluate the impact of each component, we compare our full system against two ablations: (1) CoarseNet alone (CNet) and (2) CoarseNet + RefineNet (C+RNet), which represents the full system without finger motion. The full system is denoted as C+R+FNet. This evaluation focuses on the motion synthesis quality before physics tracking. We present the evaluation for the physics tracker in Sec. 7.3.

**Results.** The qualitative comparison in Fig. 5 clearly demonstrates the superiority of our method. Both ablated variants show a lack of finger detail, and GRIP [48] fails to generate accurate hand motion, resulting in significant artifacts. In contrast, our method produces precise finger-object interactions. We also observe the impact of RefineNet: compared to CNet, C+RNet maintains more consistent and reasonable relative poses between the hand and object during the interaction, showing RefineNet’s role in improving pose consistency and reducing artifacts.

The quantitative results are presented in Tab. 1. Since our method focuses on finger-object interaction, the five metrics under the *Interaction* column are particularly important, and we achieve the best performance across all of them.

We further conduct a human perception study to complement our evaluation. We generate 15 sequences using each method and compose 60 pairs, with each pair consisting of our results and the results of a baseline. Each pair was reviewed by 20 Amazon Mechanical Turk (AMT) workers. As shown in Fig. 6, our method is consistently preferred over the baselines by a large margin. Notably, our method achieves even higher preference rates when compared to the real-world data from the FullBodyManipulation [26] dataset, as we generate detailed finger motions that are absent in the original dataset.

### 7.3. Evaluation of Physics Tracker

The physics tracker can accurately track kinematic motion while ensuring the physical plausibility of the motion. Through physics simulation, artifacts such as foot floating, foot sliding, and human-object penetration are eliminated, as shown in Fig. 7.

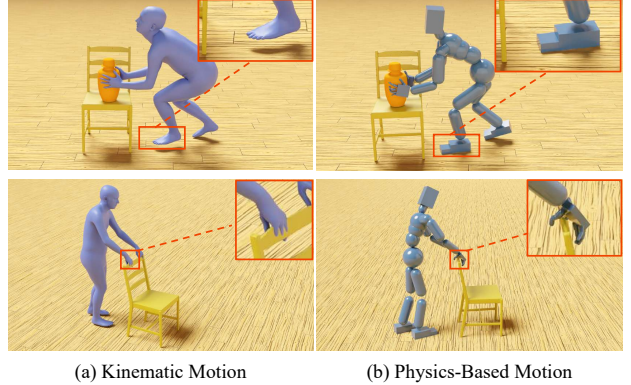


Figure 7. Qualitative comparison of kinematic motion and physics-based motion. The physics tracker corrects artifacts such as foot floating and penetration.

Additionally, we evaluate the tracking error of human joints ( $E_h$ ) and objects ( $E_o$ ), as shown in Tab. 3. The tracking error is defined as the positional error (cm) between the kinematic motion and the tracked motion. The results were evaluated across 20

Table 3. Tracking error between the kinematic motion and physics-based motion.

|      | $E_h$ | $E_o$ |
|------|-------|-------|
| Ours | 5.45  | 4.67  |

interaction sequences, each with an average duration of 30 seconds and 2 objects of varying shapes and types. All sequences were successfully tracked, with relatively small errors, demonstrating high tracking accuracy.

## 8. Conclusions

In this work, we introduced a system that simulates realistic human-object manipulation in a contextual environment based on human-level language instructions. The framework consists of a high-level LLM planner that infers a target scene layout and execution plan from the given instructions, a low-level motion generator that generates synchronized, full-body, fingers, and object motion, and a physics tracker that imitates the generated kinematic motions and produces physically plausible interaction motions. Our system effectively handles a variety of tasks, showcasing its potential for various real-world applications.

**Future Work.** Our system currently uses text or image inputs to represent the contextual environment, and could potentially be enhanced with more structured representations like voxel grids as used in [20]. Building on this idea, a promising direction is to create an agent with egocentric vision perception as input to LLM/VLMs for high-level motion planning. This could enable the agent to exhibit more natural behaviors, such as purposeful head orientation for observation and better body positioning to avoid collisions.



**Acknowledgement.** We thank Wenyang Zhou for data processing. This work is in part supported by the Wu Tsai Human Performance Alliance at Stanford University and the Stanford Institute for Human-Centered AI (HAI).

## References

- [1] Rio Aguina-Kang, Maxim Gumin, Do Heon Han, Stewart Morris, Seung Jean Yoo, Aditya Ganeshan, R Kenny Jones, Qiuhong Anna Wei, Kailiang Fu, and Daniel Ritchie. Open-universe indoor scene generation using llm program synthesis and uncurated object databases. *arXiv preprint arXiv:2403.09675*, 2024. 2, 3
- [2] Joao Pedro Araujo, Jiaman Li, Karthik Vetrivel, Rishi Agarwal, Deepak Gopinath, Jiajun Wu, Alexander Clegg, and C Karen Liu. Circle: Capture in rich contextual environments. In *Conference on Computer Vision and Pattern Recognition (CVPR)*, 2023. 2
- [3] Samarth Brahmabhatt, Ankur Handa, James Hays, and Dieter Fox. Contactgrasp: Functional multi-finger grasp synthesis from contact. In *2019 IEEE/RSJ International Conference on Intelligent Robots and Systems (IROS)*, pages 2386–2393. IEEE, 2019. 2, 4
- [4] Jona Braun, Sammy Christen, Muhammed Kocabas, Emre Aksan, and Otmar Hilliges. Physically plausible full-body hand-object interaction synthesis. *arXiv preprint arXiv:2309.07907*, 2023. 2
- [5] Sammy Christen, Shreyas Hampali, Fadime Sener, Edoardo Remelli, Tomas Hodan, Eric Sauser, Shugao Ma, and Bugra Tekin. Diffh2o: Diffusion-based synthesis of hand-object interactions from textual descriptions. *arXiv preprint arXiv:2403.17827*, 2024. 2
- [6] Christian Diller and Angela Dai. Cg-hoi: Contact-guided 3d human-object interaction generation. *arXiv preprint arXiv:2311.16097*, 2023. 2
- [7] Yan Ding, Xiaohan Zhang, Chris Paxton, and Shiqi Zhang. Task and motion planning with large language models for object rearrangement. In *2023 IEEE/RSJ International Conference on Intelligent Robots and Systems (IROS)*, pages 2086–2092. IEEE, 2023. 3
- [8] Zicong Fan, Omid Taheri, Dimitrios Tzionas, Muhammed Kocabas, Manuel Kaufmann, Michael J. Black, and Otmar Hilliges. ARCTIC: A dataset for dexterous bimanual hand-object manipulation. In *Conference on Computer Vision and Pattern Recognition (CVPR)*, 2023. 2
- [9] Anindita Ghosh, Rishabh Dabral, Vladislav Golyanik, Christian Theobalt, and Philipp Slusallek. Imos: Intent-driven full-body motion synthesis for human-object interactions. In *Eurographics*, 2023. 7, 8
- [10] Anindita Ghosh, Rishabh Dabral, Vladislav Golyanik, Christian Theobalt, and Philipp Slusallek. Imos: Intent-driven full-body motion synthesis for human-object interactions. In *Computer Graphics Forum*, pages 1–12. Wiley Online Library, 2023. 2
- [11] Patrick Grady, Chengcheng Tang, Christopher D Twigg, Minh Vo, Samarth Brahmabhatt, and Charles C Kemp. Contactopt: Optimizing contact to improve grasps. In *Proceedings of the IEEE/CVF Conference on Computer Vision and Pattern Recognition*, pages 1471–1481, 2021. 7
- [12] Chuan Guo, Shihao Zou, Xinxin Zuo, Sen Wang, Wei Ji, Xingyu Li, and Li Cheng. Generating diverse and natural 3d human motions from text. In *Proceedings of the IEEE/CVF Conference on Computer Vision and Pattern Recognition*, pages 5152–5161, 2022. 7, 5
- [13] Mohamed Hassan, Vasileios Choutas, Dimitrios Tzionas, and Michael J Black. Resolving 3d human pose ambiguities with 3d scene constraints. In *International Conference on Computer Vision (ICCV)*, pages 2282–2292, 2019. 2
- [14] Mohamed Hassan, Duygu Ceylan, Ruben Villegas, Jun Saito, Jimei Yang, Yi Zhou, and Michael Black. Stochastic scene-aware motion prediction. In *International Conference on Computer Vision (ICCV)*, pages 11354–11364, 2021. 2
- [15] Mohamed Hassan, Yunrong Guo, Tingwu Wang, Michael Black, Sanja Fidler, and Xue Bin Peng. Synthesizing physical character-scene interactions. In *SIGGRAPH 2023 Conference Papers*, 2023. 2
- [16] Yining Hong, Haoyu Zhen, Peihao Chen, Shuhong Zheng, Yilun Du, Zhenfang Chen, and Chuang Gan. 3d-llm: Injecting the 3d world into large language models. *Advances in Neural Information Processing Systems*, 36:20482–20494, 2023. 2, 3
- [17] Yingdong Hu, Fanqi Lin, Tong Zhang, Li Yi, and Yang Gao. Look before you leap: Unveiling the power of gpt-4v in robotic vision-language planning. *arXiv preprint arXiv:2311.17842*, 2023. 3
- [18] Siyuan Huang, Zan Wang, Puhao Li, Baoxiong Jia, Tengyu Liu, Yixin Zhu, Wei Liang, and Song-Chun Zhu. Diffusion-based generation, optimization, and planning in 3d scenes. In *Conference on Computer Vision and Pattern Recognition (CVPR)*, 2023. 2
- [19] Hanwen Jiang, Shaowei Liu, Jiashun Wang, and Xiaolong Wang. Hand-object contact consistency reasoning for human grasps generation. In *Proceedings of the IEEE/CVF international conference on computer vision*, pages 11107–11116, 2021. 2
- [20] Nan Jiang, Zimo He, Zi Wang, Hongjie Li, Yixin Chen, Siyuan Huang, and Yixin Zhu. Autonomous character-scene interaction synthesis from text instruction. *arXiv preprint arXiv:2410.03187*, 2024. 8
- [21] Nan Jiang, Zhiyuan Zhang, Hongjie Li, Xiaoxuan Ma, Zan Wang, Yixin Chen, Tengyu Liu, Yixin Zhu, and Siyuan Huang. Scaling up dynamic human-scene interaction modeling. *arXiv preprint arXiv:2403.08629*, 2024. 2
- [22] Justin Johnson, Ranjay Krishna, Michael Stark, Li-Jia Li, David Shamma, Michael Bernstein, and Li Fei-Fei. Image retrieval using scene graphs. In *Proceedings of the IEEE conference on computer vision and pattern recognition*, pages 3668–3678, 2015. 3
- [23] Korrawe Karunratanakul, Jinlong Yang, Yan Zhang, Michael J Black, Krikamol Muandet, and Siyu Tang. Grasping field: Learning implicit representations for human grasps. In *2020 International Conference on 3D Vision (3DV)*, pages 333–344. IEEE, 2020. 2
- [24] Diederik P Kingma and Jimmy Ba. Adam: A method for stochastic optimization. In *International Conference on Learning Representations (ICLR)*, 2015. 3

- [25] Jiaman Li, Alexander Clegg, Roozbeh Mottaghi, Jiajun Wu, Xavier Puig, and C Karen Liu. Controllable human-object interaction synthesis. *arXiv preprint arXiv:2312.03913*, 2023. 1, 2, 4, 7, 8, 5
- [26] Jiaman Li, Jiajun Wu, and C Karen Liu. Object motion guided human motion synthesis. *ACM Trans. Graph.*, 42(6), 2023. 2, 7, 8
- [27] Quanzhou Li, Jingbo Wang, Chen Change Loy, and Bo Dai. Task-oriented human-object interactions generation with implicit neural representations. In *Proceedings of the IEEE/CVF Winter Conference on Applications of Computer Vision*, pages 3035–3044, 2024. 7, 8
- [28] Ying Li, Jiaxin L Fu, and Nancy S Pollard. Data-driven grasp synthesis using shape matching and task-based pruning. *IEEE Transactions on Visualization and Computer Graphics*, 13(4): 732–747, 2007. 2
- [29] Haotian Liu, Chunyuan Li, Qingyang Wu, and Yong Jae Lee. Visual instruction tuning. *Advances in neural information processing systems*, 36, 2024. 2
- [30] Libin Liu and Jessica Hodgins. Learning basketball dribbling skills using trajectory optimization and deep reinforcement learning. *ACM Transactions on Graphics (TOG)*, 37(4):1–14, 2018. 3
- [31] Xueyi Liu and Li Yi. Geneoh diffusion: Towards generalizable hand-object interaction denoising via denoising diffusion. *arXiv preprint arXiv:2402.14810*, 2024. 2
- [32] Zhengyi Luo, Jinkun Cao, Sammy Christen, Alexander Winkler, Kris Kitani, and Weipeng Xu. Grasping diverse objects with simulated humanoids. *arXiv preprint arXiv:2407.11385*, 2024. 1, 3, 4
- [33] Viktor Makoviychuk, Lukasz Wawrzyniak, Yunrong Guo, Michelle Lu, Kier Storey, Miles Macklin, David Hoeller, Nikita Rudin, Arthur Allshire, Ankur Handa, and Gavriel State. Isaac gym: High performance gpu-based physics simulation for robot learning, 2021. 3
- [34] Aymen Mir, Xavier Puig, Angjoo Kanazawa, and Gerard Pons-Moll. Generating continual human motion in diverse 3d scenes. *arXiv preprint arXiv:2304.02061*, 2023. 2
- [35] OpenAI. Hello gpt-4o, 2024. 6
- [36] R OpenAI. Gpt-4 technical report. arxiv 2303.08774. *View in Article*, 2(5), 2023. 2
- [37] Georgios Pavlakos, Vasileios Choutas, Nima Ghorbani, Timo Bolkart, Ahmed A. A. Osman, Dimitrios Tzionas, and Michael J. Black. Expressive body capture: 3d hands, face, and body from a single image. In *Conference on Computer Vision and Pattern Recognition (CVPR)*, pages 10975–10985, 2019. 1
- [38] Xiaogang Peng, Yiming Xie, Zizhao Wu, Varun Jampani, Deqing Sun, and Huaizu Jiang. Hoi-diff: Text-driven synthesis of 3d human-object interactions using diffusion models. *arXiv preprint arXiv:2312.06553*, 2023. 2, 3
- [39] Xue Bin Peng, Pieter Abbeel, Sergey Levine, and Michiel Van de Panne. Deepmimic: Example-guided deep reinforcement learning of physics-based character skills. *ACM Transactions On Graphics (TOG)*, 37(4):1–14, 2018. 3
- [40] Xue Bin Peng, Ze Ma, Pieter Abbeel, Sergey Levine, and Angjoo Kanazawa. Amp: Adversarial motion priors for stylized physics-based character control. *ACM Transactions on Graphics (TOG)*, 40(4):1–20, 2021. 3
- [41] Nancy S Pollard and Victor Brian Zordan. Physically based grasping control from example. In *Proceedings of the 2005 ACM SIGGRAPH/Eurographics symposium on Computer animation*, pages 311–318, 2005. 2, 5
- [42] Sergey Prokudin, Christoph Lassner, and Javier Romero. Efficient learning on point clouds with basis point sets. In *International Conference on Computer Vision (ICCV)*, pages 4332–4341, 2019. 5
- [43] Alec Radford, Jong Wook Kim, Chris Hallacy, Aditya Ramesh, Gabriel Goh, Sandhini Agarwal, Girish Sastry, Amanda Askell, Pamela Mishkin, Jack Clark, et al. Learning transferable visual models from natural language supervision. In *International conference on machine learning*, pages 8748–8763. PMLR, 2021. 5
- [44] Alberto Rodriguez, Matthew T Mason, and Steve Ferry. From caging to grasping. *The International Journal of Robotics Research*, 31(7):886–900, 2012. 2
- [45] John Schulman, Filip Wolski, Prafulla Dhariwal, Alec Radford, and Oleg Klimov. Proximal policy optimization algorithms, 2017. 6, 3
- [46] Omid Taheri, Nima Ghorbani, Michael J. Black, and Dimitrios Tzionas. GRAB: A dataset of whole-body human grasping of objects. In *European Conference on Computer Vision (ECCV)*, 2020. 2, 7, 3
- [47] Omid Taheri, Vasileios Choutas, Michael J Black, and Dimitrios Tzionas. Goal: Generating 4d whole-body motion for hand-object grasping. In *Conference on Computer Vision and Pattern Recognition (CVPR)*, pages 13263–13273, 2022. 2
- [48] Omid Taheri, Yi Zhou, Dimitrios Tzionas, Yang Zhou, Duygu Ceylan, Soren Pirk, and Michael J Black. Grip: Generating interaction poses using latent consistency and spatial cues. *arXiv preprint arXiv:2308.11617*, 2023. 6, 7, 8, 5
- [49] Purva Tendulkar, Dídac Surís, and Carl Vondrick. Flex: Full-body grasping without full-body grasps. In *Proceedings of the IEEE/CVF Conference on Computer Vision and Pattern Recognition*, pages 21179–21189, 2023. 2
- [50] Naoki Wake, Atsushi Kanehira, Kazuhiro Sasabuchi, Jun Takamatsu, and Katsushi Ikeuchi. Gpt-4v (ision) for robotics: Multimodal task planning from human demonstration. *arXiv preprint arXiv:2311.12015*, 2023. 3
- [51] Jiashun Wang, Huazhe Xu, Jingwei Xu, Sifei Liu, and Xiaolong Wang. Synthesizing long-term 3d human motion and interaction in 3d scenes. In *Conference on Computer Vision and Pattern Recognition (CVPR)*, pages 9401–9411, 2021. 2
- [52] Jingbo Wang, Yu Rong, Jingyuan Liu, Sijie Yan, Dahua Lin, and Bo Dai. Towards diverse and natural scene-aware 3d human motion synthesis. In *Conference on Computer Vision and Pattern Recognition (CVPR)*, pages 20460–20469, 2022. 2
- [53] Ruicheng Wang, Jialiang Zhang, Jiayi Chen, Yinzhen Xu, Puhao Li, Tengyu Liu, and He Wang. Dexgraspnet: A large-scale robotic dexterous grasp dataset for general objects based on simulation. In *2023 IEEE International Conference on Robotics and Automation (ICRA)*, pages 11359–11366. IEEE, 2023. 2, 5, 1

- [54] Ruocheng Wang, Pei Xu, Haochen Shi, Elizabeth Schumann, and C Karen Liu. F\” urelise: Capturing and physically synthesizing hand motions of piano performance. *arXiv preprint arXiv:2410.05791*, 2024. [3](#)
- [55] Yinhuai Wang, Jing Lin, Ailing Zeng, Zhengyi Luo, Jian Zhang, and Lei Zhang. Physshoi: Physics-based imitation of dynamic human-object interaction. *arXiv preprint arXiv:2312.04393*, 2023. [1](#), [3](#), [4](#), [5](#)
- [56] Zan Wang, Yixin Chen, Tengyu Liu, Yixin Zhu, Wei Liang, and Siyuan Huang. Humanise: Language-conditioned human motion generation in 3d scenes. In *Advances in Neural Information Processing Systems (NeurIPS)*, 2022. [2](#)
- [57] Zan Wang, Yixin Chen, Baoxiong Jia, Puhao Li, Jinlu Zhang, Jingze Zhang, Tengyu Liu, Yixin Zhu, Wei Liang, and Siyuan Huang. Move as you say, interact as you can: Language-guided human motion generation with scene affordance. *arXiv preprint arXiv:2403.18036*, 2024. [2](#)
- [58] Qianyang Wu, Ye Shi, Xiaoshui Huang, Jingyi Yu, Lan Xu, and Jingya Wang. Thor: Text to human-object interaction diffusion via relation intervention. *arXiv preprint arXiv:2403.11208*, 2024. [2](#)
- [59] Yan Wu, Jiahao Wang, Yan Zhang, Siwei Zhang, Otmar Hilliges, Fisher Yu, and Siyu Tang. Saga: Stochastic whole-body grasping with contact. In *European Conference on Computer Vision (ECCV)*, pages 257–274, 2022. [2](#)
- [60] Zeqi Xiao, Tai Wang, Jingbo Wang, Jinkun Cao, Wenwei Zhang, Bo Dai, Dahua Lin, and Jiangmiao Pang. Unified human-scene interaction via prompted chain-of-contacts. In *The Twelfth International Conference on Learning Representations*, 2024. [1](#), [2](#), [3](#)
- [61] Zhaoming Xie, Sebastian Starke, Hung Yu Ling, and Michiel van de Panne. Learning soccer juggling skills with layer-wise mixture-of-experts. In *ACM SIGGRAPH 2022 Conference Proceedings*, pages 1–9, 2022. [3](#)
- [62] Pei Xu and Ioannis Karamouzas. A gan-like approach for physics-based imitation learning and interactive character control. *Proceedings of the ACM on Computer Graphics and Interactive Techniques*, 4(3):1–22, 2021. [3](#)
- [63] Pei Xu and Ruocheng Wang. Synchronize dual hands for physics-based dexterous guitar playing. *arXiv preprint arXiv:2409.16629*, 2024. [3](#)
- [64] Sirui Xu, Ziyin Wang, Yu-Xiong Wang, and Liang-Yan Gui. Interdreamer: Zero-shot text to 3d dynamic human-object interaction. *arXiv preprint arXiv:2403.19652*, 2024. [2](#), [3](#)
- [65] Yue Yang, Fan-Yun Sun, Luca Weihs, Eli VanderBilt, Alvaro Herrasti, Winson Han, Jiajun Wu, Nick Haber, Ranjay Krishna, Lingjie Liu, et al. Holodeck: Language guided generation of 3d embodied ai environments. In *Proceedings of the IEEE/CVF Conference on Computer Vision and Pattern Recognition*, pages 16227–16237, 2024. [3](#)
- [66] Heyuan Yao, Zhenhua Song, Yuyang Zhou, Tenglong Ao, Baoquan Chen, and Libin Liu. Moconvq: Unified physics-based motion control via scalable discrete representations. *ACM Transactions on Graphics (TOG)*, 43(4):1–21, 2024. [3](#)
- [67] Yuting Ye and C Karen Liu. Synthesis of detailed hand manipulations using contact sampling. *ACM Transactions on Graphics (ToG)*, 31(4):1–10, 2012. [2](#)
- [68] Hongwei Yi, Justus Thies, Michael J Black, Xue Bin Peng, and Davis Rempe. Generating human interaction motions in scenes with text control. *arXiv preprint arXiv:2404.10685*, 2024. [2](#)
- [69] Yiming Zeng, Mingdong Wu, Long Yang, Jiyao Zhang, Hao Ding, Hui Cheng, and Hao Dong. Distilling functional rearrangement priors from large models. *arXiv preprint arXiv:2312.01474*, 2023. [3](#)
- [70] He Zhang, Yuting Ye, Takaaki Shiratori, and Taku Komura. Manipnet: neural manipulation synthesis with a hand-object spatial representation. *ACM Transactions on Graphics (ToG)*, 40(4):1–14, 2021. [2](#), [6](#), [3](#)
- [71] Xiaohan Zhang, Bharat Lal Bhatnagar, Sebastian Starke, Vladimir Guzov, and Gerard Pons-Moll. Couch: Towards controllable human-chair interactions. In *European Conference on Computer Vision (ECCV)*, pages 518–535, 2022. [2](#)
- [72] Yaqi Zhang, Di Huang, Bin Liu, Shixiang Tang, Yan Lu, Lu Chen, Lei Bai, Qi Chu, Nenghai Yu, and Wanli Ouyang. Motiongpt: Finetuned llms are general-purpose motion generators. In *Proceedings of the AAAI Conference on Artificial Intelligence*, pages 7368–7376, 2024. [3](#)
- [73] Kaifeng Zhao, Yan Zhang, Shaofei Wang, Thabo Beeler, and Siyu Tang. Synthesizing diverse human motions in 3d indoor scenes. *arXiv preprint arXiv:2305.12411*, 2023. [2](#)
- [74] Yi Zhou, Connelly Barnes, Jingwan Lu, Jimei Yang, and Hao Li. On the continuity of rotation representations in neural networks. In *Computer Vision and Pattern Recognition (CVPR)*, 2019. [4](#), [6](#)



# Human-Object Interaction from Human-Level Instructions

## Supplementary Material

### A. Details of High-Level Planner

#### A.1. Pseudo-code for Object Positions Calculation

In Algorithm 1, we provide the pseudo-code for the algorithm that calculates object positions in the scene graph, as described in Sec. 4.1.

---

**ALGORITHM 1:** Object Positions Calculation

---

**Input** : Scene graph  $G(V, E)$  with vertices  $V$  and edges  $E$ , initial positions  $L$ , static nodes ( $V_S$ ), the nodes to be moved ( $V_M$ ).

**Output** : Updated positions  $L$  for all nodes.

**Procedure** `ComputePositions( $G, L$ )` :

- Let the set of processed nodes  $V_P \leftarrow V_S$
- while**  $V_M$  is not empty **do**
  - Let  $V' \subseteq V_M$  be the nodes whose predecessors' positions are known
  - foreach**  $v \in V'$  **do**
    - $L(v) \leftarrow \text{Update}(v, G, L)$
    - $V_P \leftarrow V_P \cup \{v\}$
    - $V_M \leftarrow V_M \setminus \{v\}$
- end**
- return**  $L$

**return**

**Procedure** `Update( $v, G, L$ )` :

- Initialize an empty list of positions  $P$
- foreach** predecessor  $u$  of  $v$  in  $G$  **do**
  - $O \leftarrow \text{ComputeOffset}((u, v), L(u))$
  - Append  $L(u) + O$  to  $P$
- end**
- return** `Average( $P$ )`

**return**

**Procedure** `ComputeOffset( $(u, v), L(u)$ )` :

- if** edge  $(u, v)$  indicates “on” **then**
  - Set  $O_{\text{height}}$  to align with the top surface of  $u$
  - Sample  $O_{\text{horizontal}}$  within the horizontal bounds of  $u$
  - return**  $[O_{\text{horizontal}}, O_{\text{height}}]$
- end**
- else if** edge  $(u, v)$  indicates “adjacent” **then**
  - Use the direction and distance provided by the LLMs to compute  $O$
  - return**  $O$
- end**
- return**

---

#### A.2. Prompts for High-Level Planner

We provide the prompts used for generating the scene map and execution plan in Fig. S1. An example of the input and the corresponding output of the LLM planner is shown in Fig. S2. We also present the prompt used by the baseline (as described in Sec. 7.1) in Fig. S3.

### B. Details of Low-Level Motion Generator

#### B.1. Diffusion Model Architecture

Our system includes four diffusion models: CoarseNet, RefineNet, FingerNet, and the navigation module, all of which adopt a similar transformer-based architecture. Here, we illustrate the architecture of RefineNet in Fig. S4. The model is provided with a motion sequence  $x_n$ , the condition  $c_r$ , and the noise step  $n$ , and predicts the clean motion  $\hat{x}_0$ . For the other networks, we simply substitute the condition with the corresponding one.

#### B.2. Implementation Details of Grasp Pose Generation

As introduced in Sec. 5.2.2, we use a state-of-the-art grasp pose generation method [53] to generate the grasp pose. Although originally designed for robotic hand grasping, this method relies solely on kinematic chain information, making it fully compatible with the SMPL-X [37] hand model. Starting with an object mesh and an initial hand pose, the grasp generation process is formulated as an optimization problem that minimizes a differentiable force closure energy term along with several additional terms that encourage the fingers to conform closely to the object surface while maintaining a natural hand shape. For motions involving both hands, such as carrying a box, we omit the force closure term.

#### B.3. Post-processing in RefineNet

As introduced in Sec. 5.2.3, we apply post-processing to RefineNet’s output to better align it with the input condition. First, we replace the object poses in the pre-contact and post-contact phases with the corresponding static poses. To address the abrupt transitions at the phase boundaries, we identify the difference between the predicted object pose and the static object pose at the boundary frame denoted as  $\Delta d \in \mathbb{R}^6$  (suppose this is the boundary between pre-contact phase and contact phase), which encapsulates both the positional and rotational differences in axis-angle format. To smooth these transitions, we employ an interpolation strategy to the object motion in the contact phase. The interpolation function is defined by  $\hat{O}_t = O_t + \alpha_t \Delta d$ , where  $\alpha_t$  is a time-dependent scaling fac-

**Scene Map Generation Prompt:** I will provide a scene description outlining the current layout of a room, along with instructions on how it should be rearranged. Your task is to create a detailed target layout based on these descriptions. When describing the target layout, please:

1. Identify the objects involved in the rearrangement, including those that need to be moved and those necessary to define the spatial relationships.
2. Specify the precise spatial relationships between objects in the target layout.

[start of rules]

1. When describing spatial relationships, use only the following relationships:
  - a. on: Signifies that object A is on top of object B.
  - b. adjacent: Indicates that object A is near object B. You may also describe the direction between them, using terms like east, west, south, and north. And you can also specify the distance between them.
  - c. facing: Denotes that object A is facing object B. When the direction is not important or can be arbitrary, say "with no specific facing direction".
2. List all relevant position and orientation relationships for all objects involved.
3. Avoid describing spatial relationships between objects that aren't involved in this rearrangement process.

[end of rules]

**Execution Plan Generation Prompt:** Determine the most natural order to move each object to achieve the target layout. Give a reason for your choice.

[start of rules]

1. You can move one object at a time.
2. You shouldn't move an object more than once.
3. You cannot move an object if there is currently another object on top of it.

[end of rules]

Figure S1. Prompts used by the LLM planner to generate the scene map and execution plan.

**Input:**

**Scene description:** The room contains static objects: [table], and movable objects: [chair, monitor]. The table has space only on its south side for placing items, as the other directions are obstructed. Below is the information about the objects, with all center-of-mass values representing the height of the object when it is placed on the ground:

- The height of the table is 0.8 meters.
- The center of mass of the chair is at 0.5 meters.
- The center of mass of the monitor is at 0.3 meters.

The following are the positions of the objects in the initial layout:

- The table is at position (2.0, 1.0, 0.5).

The dimensions of the objects:

- The table has an XY bounding box of 1.2 meters in the X direction and 1.0 meter in the Y direction.

For orientation:

- North corresponds to the XY direction (1,0),
- South corresponds to (-1,0),
- East corresponds to (0,-1),
- West corresponds to (0,1).

**Instruction:** I want to set up my workspace.

**Output:**

**Scene Map:**

Monitor: {(2.0, 1.0, 0.8), south},  
 Chair: {(0.4, 1.0, 0.5), north}.

**Execution Plan:**

1. Lift the monitor, move the monitor, put down the monitor.
2. Lift the chair, move the chair, put down the chair.

Figure S2. Example of the input and output for the LLM planner.

tor that decreases from 1 to 0 across the transition period,  $O_t$  denotes the predicted object pose.

Next, we use the rectified object motion and the optimized wrist pose  $\hat{w} = (\hat{R}, \hat{T})$  to compute the wrist trajectories during the contact phase. The rotation is computed as  $R_o \hat{R}$ , and the position is computed as  $R_o \hat{T} + T_o$ , where  $R_o$  and

$T_o$  represent the object's rotation and position, respectively. The computed wrist trajectories may slightly deviate from the predicted wrist trajectories in the contact phase, leading to unsmooth transitions near the phase boundaries. We apply the same interpolation strategy to the wrist poses in the pre-contact and post-contact phases to produce smooth wrist motions.

**Scene Map Generation Prompt:** I will provide a scene description outlining the current layout of a room, along with instructions on how it should be rearranged. Your task is to create a detailed target layout based on these descriptions. When describing the target layout, please:

1. Identify the objects that need to be moved.
2. Specify the precise 3D position and orientation for those objects in the target layout.

Figure S3. Prompts used by the baseline, as described in Sec. 7.1.

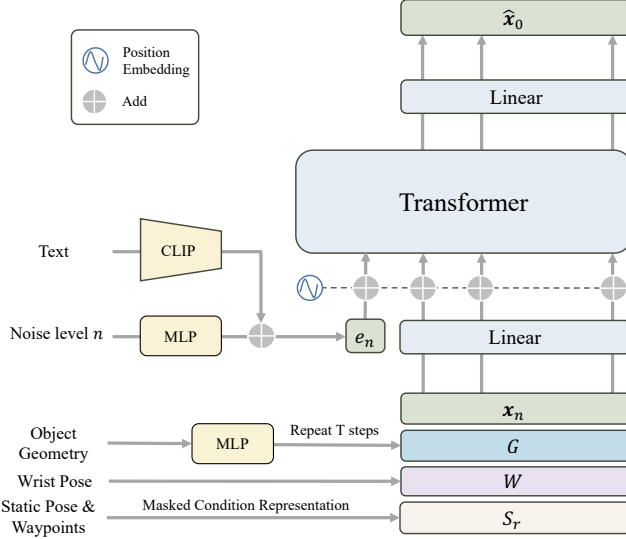


Figure S4. Architecture of RefineNet. The model is conditioned on  $c_r = \{W, S_r, G, T\}$ , where  $W$  represents the wrist-object relative pose,  $S_r$  is the masked motion representation containing the static pose and waypoints,  $G$  denotes the object geometry, and  $T$  is the textual input.

Finally, we employ an Inverse Kinematics (IK) algorithm to solve for the updated human pose constrained by the wrist poses.

#### B.4. Implementation Details of FingerNet

FingerNet generates finger motions for the pre-contact and post-contact phases to create natural transitions between rest and grasp poses. It is trained on the GRAB dataset [46]. Since FingerNet focuses solely on the hand approaching and releasing motions, we only use the corresponding portions of the dataset. Specifically, we extract one second of motion before the grasp begins and after it ends as training data, discarding the rest.

We adopt a mirroring strategy similar to [70] to handle both hands simultaneously. During training, left-hand data are mirrored and combined with the right-hand data so that the model only needs to predict motions for the right hand. At inference time, we mirror the left-hand input, predict the corresponding motions using the model, and then mirror the output back to obtain the left-hand motions.

#### B.5. Smooth Transition between Navigation and Interaction

The navigation and interaction modules alternate to generate a long-horizon interaction sequence. Specifically, when the human is far from the object, the navigation module is activated to guide the human towards it. Once the human is within a threshold distance (set at 1 meter), the system switches to the interaction module to begin object manipulation. After the interaction is completed and the object is put down, control reverts to the navigation module to move towards the next object.

Since both modules use the initial human pose as an input condition, we ensure a smooth transition by feeding the last pose from the previous module into the next. We apply the same smoothing technique described in Sec. B.3 at the switching boundary to further enhance continuity.

### C. Implementation Details of Physics Tracker

We use IsaacGym [33] as the physics engine to perform simulation. The simulated character is skeleton-driven where each joint is modeled as a motor controlled through a PD controller. The control policy works at 30Hz, which is the same with generated kinematics motions, while the simulation runs at 120Hz. Our character has 62 body links and 49 controllable joints. This results in a state space  $s_t \in \mathbb{R}^{(62+|\mathcal{O}|) \times 13}$  including the position, orientation and linear and angular velocities of the character's body links and the manipulating objects  $\mathcal{O}$  depending on the given tracking motions. To track the target motion, additional observation  $o_t \in \mathbb{R}^{(62+|\mathcal{O}|) \times 7}$  including the target position and orientation of each body link and object is also introduced as the input to the control policy. The action space is  $a_t \in \mathbb{R}^{49 \times 3}$  given each controllable joint has 3 degrees of freedom. All our control policies are optimized using PPO [45] as the backbone reinforcement learning algorithm with network parameters updated by Adam optimizers [24]. The hyperparameters used for policy training are listed in Tab. S2.

#### C.1. Reward Design

Since fingers take 30 out of 49 controllable joints and have a higher requirement in control precision for accurate object manipulation, we define a reward function containing three terms to evaluate the full-body pose and finger pose separately:



| Body Part     | Value                  |
|---------------|------------------------|
| root (pelvis) | $w_q = 1, w_p = 1$     |
| lower abdomen | $w_q = 0.2$            |
| upper abdomen | $w_q = 0.2$            |
| chest         | $w_q = 0.2$            |
| neck          | $w_q = 0.2$            |
| head          | $w_q = 0.2$            |
| clavicles     | $w_q = 0.1$            |
| upper arms    | $w_q = 0.2$            |
| lower arms    | $w_q = 0.2$            |
| wrists        | $w_q = 0.3, w_p = 0.3$ |
| thighs        | $w_q = 0.5$            |
| calfs         | $w_q = 0.3$            |
| feet          | $w_q = 0.2, w_p = 0.1$ |
| target object | $w_q = 1, w_p = 1$     |

Table S1. Unnormalized weights of each body link of the character and the target object when computing the reward regarding body pose errors (cf.  $r_{\text{body}}$  in Equation S2). All weights unlisted are zero. The weights are normalized such that  $\sum_b w_{p,b} = 1$  and  $\sum_b w_{q,b} = 1$  before computing  $r_{\text{body}}$ .

| Parameter                           | Value              |
|-------------------------------------|--------------------|
| policy network learning rate        | $5 \times 10^{-6}$ |
| critic network learning rate        | $1 \times 10^{-4}$ |
| reward discount factor ( $\gamma$ ) | 0.95               |
| GAE discount factor ( $\lambda$ )   | 0.95               |
| surrogate clip range ( $\epsilon$ ) | 0.2                |
| number of PPO workers               |                    |
| (simulation environment instances)  | 2048               |
| PPO replay buffer size              | $2048 \times 8$    |
| PPO batch size                      | 256                |
| PPO optimization epochs             | 5                  |

Table S2. Hyperparameters of policy training for physics tracker.

$$r = 0.8r_{\text{body}} + 0.2r_{\text{hand}} + 0.05r_{\text{energy}}, \quad (\text{S1})$$

where  $r_{\text{body}}$  evaluates the full-body poses excluding fingers,  $r_{\text{hand}}$  evaluates the hand poses related to the target manipulating object, and  $r_{\text{energy}}$  is an additional energy-related term penalizing end effectors' abrupt movement. Note that in our implementation, at any time step, at most one object is activated as the manipulation target, while multiple objects may exist in the scene and would be manipulated one by one.

For full-body pose evaluation, we consider the orientation and position accuracy of the character's body links and the

target object:

$$r_{\text{body}} = 0.5 \exp \left( -15 \sum_{b \in \mathcal{B}} w_{q,b} \|\mathbf{e}_{q,b}\|^2 \right) + 0.5 \exp \left( -15 \sum_{b \in \mathcal{B}} w_{p,b} \|\mathbf{e}_{p,b}\|^2 \right), \quad (\text{S2})$$

where  $\mathcal{B}$  is the set of all body links of the character and the activated target object at the current time step,  $\mathbf{e}_{q,b}$  is the orientation error between each body link  $b$  of the simulated character and that in the tracking motion,  $\mathbf{e}_{p,b}$  is the position error, and  $w_{q,b}$  and  $w_{p,b}$  are the associated weights. We measure  $\mathbf{e}_{q,b}$  using the radian of the angle needed to rotate the link  $b$  to the target orientation, while  $\mathbf{e}_{p,b}$  is measured by the Euclidean distance from the current position of link  $b$  to the target position. All weight values are listed in Tab. S1. For position tracking, we focus only on the position of the root link and end effectors to ensure that the trajectory of end effectors (foot and hand excluding fingers) matches the tracking target, while relying on orientation tracking to ensure the naturalness of full-body poses.

For hand pose evaluation, to ensure that the object would be manipulated by hands correctly, we consider the fingers' relative position to the target manipulating object when the hand is close to the object, or their relative position to the wrist when the hand is far away from the target object:

$$r_{\text{hand}} = \exp \left( -\frac{5}{|\mathcal{F}|} \sum_{f \in \mathcal{F}} \alpha \|\mathbf{e}_{f,o}\| + (1 - \alpha) \|\mathbf{e}_{f,w}\| \right), \quad (\text{S3})$$

where  $\mathcal{F}$  is the set of fingers,  $\mathbf{e}_{f,o}$  is the position error between each finger  $f$  of the simulated character and the tracking target position in the object's local system,  $\mathbf{e}_{f,w}$  is the position error in the wrist's local system, and  $\alpha$  is an interpolation coefficient depending on the distance between the hand and object in the generated tracking motions. We define  $\alpha = 1$  when the hand is equal to or less than 0.25m from the target object and  $\alpha = 0$  if the hand is at least 1m far away from the object in the tracking motion.

$r_{\text{energy}}$  takes into account the character's end effectors to prevent jittering or abrupt movement with larger acceleration:

$$r_{\text{energy}} = \exp \left( -\frac{1}{900} \sum_{e \in \mathcal{E}} \|\mathbf{a}_e\|^2 \right), \quad (\text{S4})$$

where  $\mathcal{E}$  is the set of the character's key end effectors (feet and hands excluding fingers), and  $\mathbf{a}_e$  is the linear acceleration of the end effector  $e$ .

In contrast to recent works [3, 32, 55] on object manipulation, our reward function does not rely on the contact states between the hands (or fingers) and objects. This is because the contact data derived from the kinematic motions generated by diffusion models can be unreliable due to artifacts

(cf. Fig. 7). Moreover, this approach aligns with the common scenario in which detailed contact information is typically absent in motions obtained from motion capture and video demonstrations [41].

## C.2. Importance Sampling Strategy

Given that the generated kinematic motions can span several minutes and involve interactions with multiple objects, it would be highly inefficient to perform motion tracking from the very beginning of the sequence. Since locomotion without object manipulation and the phase following object grasping are relatively easier to learn, we adopt an importance sampling strategy that focuses on pre-grasp states to facilitate policy training. Specifically, we partition the parallel simulated physics environments into  $|\mathcal{O}|$  batches, with each batch assigned to a specific manipulating object. In each batch, simulated characters are initialized in a random pre-grasp pose while interacting with the assigned object. This approach increases the likelihood that the policy learns the transition from the pre-grasp to the grasping phase, and subsequently, the locomotion that follows a successful grasp. Moreover, this strategy ensures that the policy consistently learns to interact with multiple objects simultaneously, thereby avoiding potential local minima during policy exploration.

## D. Inference Speed

Achieving real-time performance remains an open challenge for both diffusion-based and optimization-based methods. In our low-level motion generator, producing a 4-second motion sequence takes about four seconds for each diffusion model in stages 1, 3, and 4, while the optimization process in stage 2 requires roughly three minutes. Additionally, training the physics tracker on a 4-second interaction segment takes approximately 2 hours. All experiments were run on a single NVIDIA RTX 4000 GPU.

## E. Additional Experimental Analysis

### E.1. Implementation Details of Baseline

Since no prior work addresses the task of generating full-body motion, finger motion, and object motion from language instructions, we adapt prior works CHOIS [25] and GRIP [48] as fair baselines to compare against our system. CHOIS generates full-body motion and object motion from text and initial states, which also serves as our Stage 1. The output of CHOIS will serve as input to GRIP. GRIP consists of an arm denoising model and a two-stage finger motion generation model. It takes full-body motion (without finger motion) and object motion as input to denoise arm motion. It then proposes a hand sensor to extract hand-object spatial features and predict initial finger poses. In the second stage of finger motion generation, GRIP leverages these predicted finger poses to compute

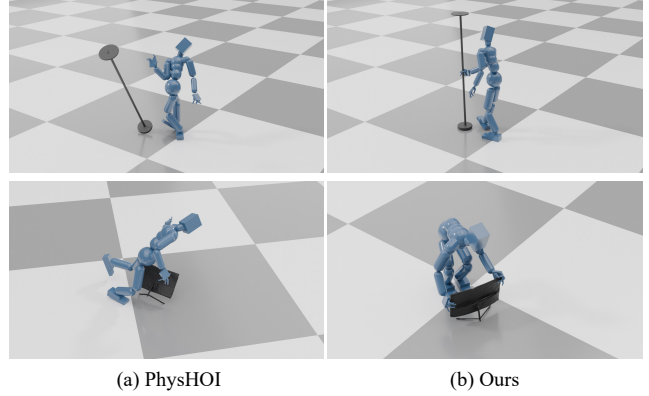


Figure S5. PhysHOI [55] fails to track kinematic motion, while our policy successfully drives the character to interact with diverse objects.

|      | $T_{xy}$ | $H_{\text{feet}}$ | $FS$ | MPJPE |
|------|----------|-------------------|------|-------|
| Ours | 4.00     | 1.48              | 0.58 | 10.87 |

Table S3. Navigation synthesis on the HumanML3D dataset [12]. The joint error is relatively small, demonstrating that the model aligns well with the input waypoints.

proximity features, which serve as input to refine the finger motion.

### E.2. Results of Navigation Module

We report the evaluation scores for the navigation module in Tab. S3, using the metrics introduced in Sec. 7.2. The module is evaluated on the test split of the HumanML3D dataset [12]. It demonstrates that the module closely adheres to the input waypoints, with a relatively small joint position error when compared to the ground truth data, while maintaining reasonable foot sliding and foot height.

### E.3. Results of Physics Tracker

We compare our physics tracker against PhysHOI [55], which trains reinforcement learning policies to control a humanoid character playing basketball. For our task, we have PhysHOI track the kinematic motion generated by our low-level motion generator. As shown in Fig. S5, PhysHOI fails to grasp objects, whereas our method successfully completes the task.

### E.4. Human Perception Study Details

We show the interface of the human perceptual study for the high-level planner in Figure S6 and the low-level motion generator in Figure S7.

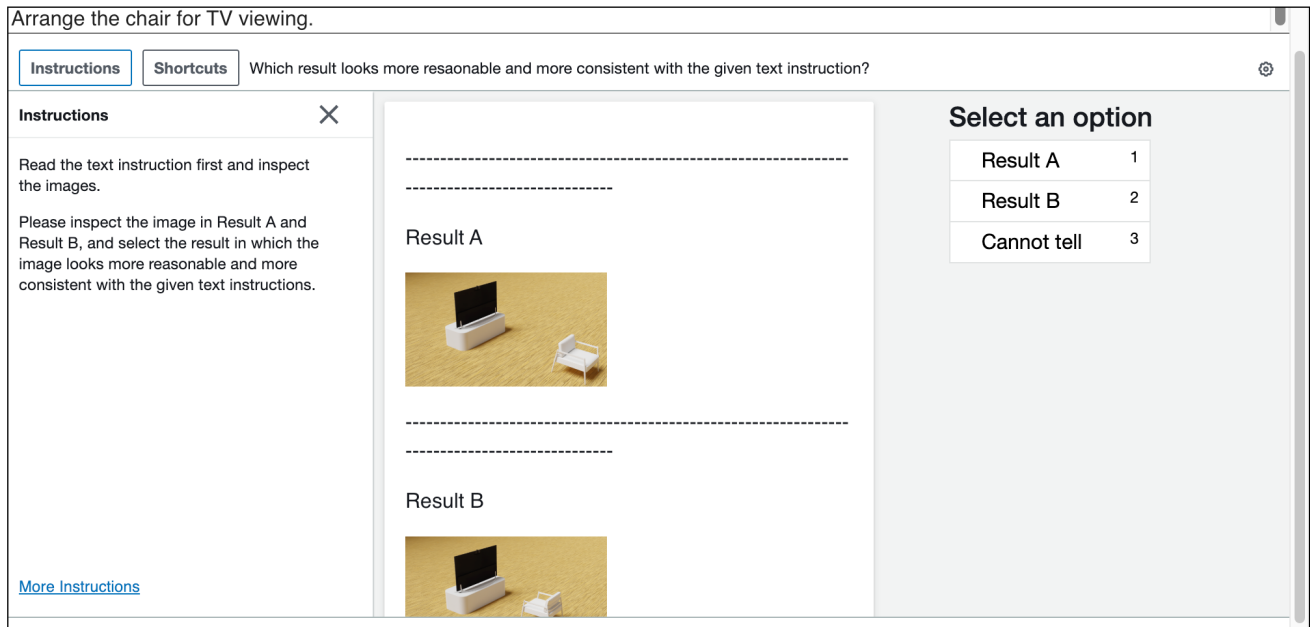


Figure S6. Interface of human perceptual study for the high-level planner.

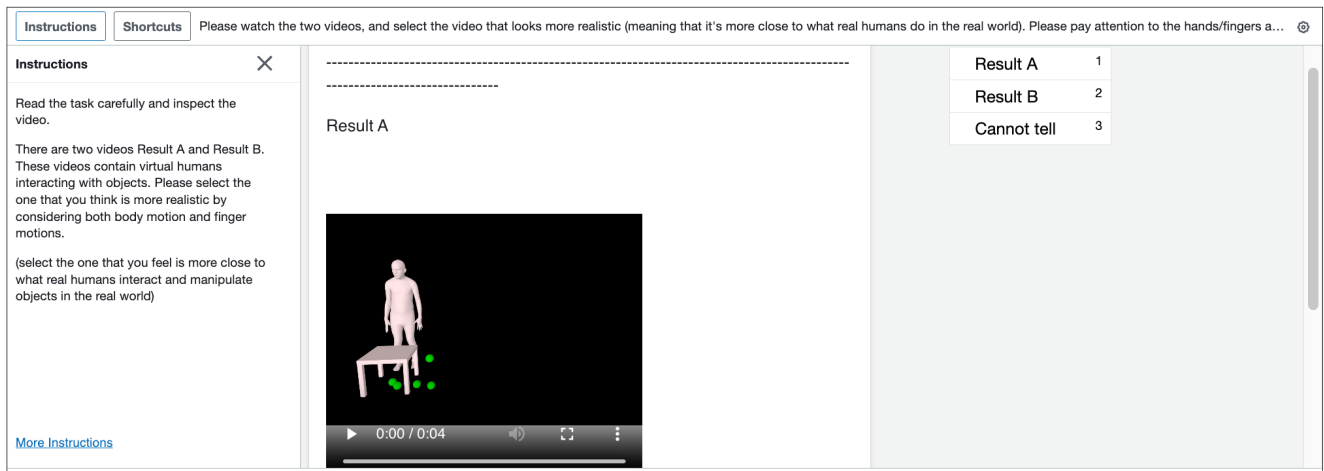


Figure S7. Interface of human perceptual study for the low-level motion generator.